

Manuscript version: Author's Accepted Manuscript

The version presented in WRAP is the author's accepted manuscript and may differ from the published version or Version of Record.

Persistent WRAP URL:

<http://wrap.warwick.ac.uk/112157>

How to cite:

Please refer to published version for the most recent bibliographic citation information. If a published version is known of, the repository item page linked to above, will contain details on accessing it.

Copyright and reuse:

The Warwick Research Archive Portal (WRAP) makes this work by researchers of the University of Warwick available open access under the following conditions.

Copyright © and all moral rights to the version of the paper presented here belong to the individual author(s) and/or other copyright owners. To the extent reasonable and practicable the material made available in WRAP has been checked for eligibility before being made available.

Copies of full items can be used for personal research or study, educational, or not-for-profit purposes without prior permission or charge. Provided that the authors, title and full bibliographic details are credited, a hyperlink and/or URL is given for the original metadata page and the content is not changed in any way.

Publisher's statement:

Please refer to the repository item page, publisher's statement section, for further information.

For more information, please contact the WRAP Team at: wrap@warwick.ac.uk.

Cryptanalyzing an image encryption algorithm based on autoblocking and electrocardiography

Chengqing Li^{a,*}, Dongdong Lin^a, Jinhu Lü^b, Feng Hao^c

^a*School of Computer Science and Electronic Engineering, Hunan University, Changsha 410082, Hunan, China*

^b*Academy of Mathematics and Systems Sciences, Chinese Academy of Sciences, Beijing 100190, China*

^c*School of Computing Science, Newcastle University, Newcastle Upon Tyne NE1 7RU, UK*

Abstract

This paper analyzes the security of an image encryption algorithm proposed by Ye and Huang [*IEEE MultiMedia*, vol. 23, pp. 64-71, 2016]. The Ye-Huang algorithm uses electrocardiography (ECG) signals to generate the initial key for a chaotic system and applies an autoblocking method to divide a plain image into blocks of certain sizes suitable for subsequent encryption. The designers claimed that the proposed algorithm is “strong and flexible enough for practical applications”. In this paper, we perform a thorough analysis of their algorithm from the view point of modern cryptography. We find it is vulnerable to the known plaintext attack: based on one pair of a known plain-image and its corresponding cipher-image, an adversary is able to derive a mask image, which can be used as an equivalent secret key to successfully decrypt other cipher-images encrypted under the same key with a non-negligible probability of 1/256. Using this as a typical counterexample, we summarize security defects in the design of the Ye-Huang algorithm. The lessons are generally applicable to many other image encryption schemes.

Keywords: Known-plaintext attack, cryptanalysis, image encryption, chaotic cryptography, image privacy.

1. Introduction

Security and privacy of image data have become almost everyone’s concern as sharing and enjoying photos on social media are a part of our daily lives nowadays, which is strongly supported by human’s complex emotional needs, e.g., narcissism, popularity and belongingness. To cope with the challenges, a great number of image encryption and privacy protection schemes were proposed to conceal important information about the original image data from the unintended viewers [1, 2, 3]. The complex dynamics of chaotic maps demonstrated in an infinite-precision world are similar to the required properties of a secure encryption system initially summarized by Shannon, the father of information theory, in the late 1940s [4, Table 1]. The similarity attracts many security researchers to utilize various chaotic systems and methodologies for all kinds of cryptographic applications, including image encryption, video encryption, image privacy protection, public key infrastructure and hash. Some biometric personal features, e.g. fingerprint, iris, and

electrocardiography (ECG) signals, are used for identification and cryptography in various application scenarios, e.g. Internet of Things [5].

ECG records electrical changes of the skin arising from the heart muscle’s electrophysiologic patterns of depolarization and repolarization during each heartbeat. The dynamic properties of the time series of ECG, measured by the 2D degree distribution of the corresponding complex networks, can be used as a tool to identify healthy persons from pathological groups. In different cryptographic scenarios, the ECG signal is used for various purposes. In [6], its characteristics in Fourier domain are used as a key for realizing secure communication and hash-based authentication among sensor nodes in a body area sensor networks (BANs). To assure an ECG signal is securely transmitted in BANs, it is first compressed with a compression algorithm called SPIHT (set partitioning in hierarchical trees) and then a small portion of important coefficients in the compression domain are encrypted using a well-known modern cipher [7]. The importance of the compression coefficients is evaluated in terms of their influence strength on decompression. To keep a patient’s ECG information private in an automatic online diagnosis system identifying

*Corresponding author.

Email address: DrChengqingLi@gmail.com (Chengqing Li)

six possible states of heart beat, four feature coefficients of the ECG signal are extracted and encrypted by a homomorphic encryption scheme before transmission to the system [8]. In [9], a feature extraction technique of ECG is proposed to accurately authenticate whether two ECG signals belong to the same person.

In [10], a personalized information encryption scheme using ECG signals with chaotic functions was proposed. In this scheme, the Lyapunov exponent of an ECG signal is used as the initial states of two pseudorandom number generators composed of a logistic map and a Henon map, respectively. As selection of chaotic map is a core step in the design of a chaos-based cryptosystem, some unimodal maps like logistic map can weaken security of the supported cryptosystem [11]. In addition, dynamics of any chaotic map in the digital domain are degenerated and may seriously influence the security of the supporting encryption function [12, 13]. The paper [10] skipped the problem and did not provide any information on the concrete functions used for diffusion and confusion, which violates some basic design principles summarized in [4]. To improve the scheme proposed in [10], Ye and Huang proposed an image encryption algorithm based on autoblocking and electrocardiography (IEAE) in [14]. Their method is to use an ECG signal to generate the initial keys to control the whole encryption process composed of block-wise matrix multiplications. This paper re-evaluates the security of IEAE and we find that IEAE is susceptible to a known-plaintext attack. In addition, the security defects in IEAE are summarized, along with lessons for avoiding similar pitfalls in the design of image encryption schemes.

The rest of the paper is organized as follows. Section 2 presents a description of IEAE. Detailed cryptanalytic results on IEAE are given in Section 3. The last section concludes the paper.

2. Image encryption algorithm based on autoblocking and electrocardiography (IEAE)

The encryption object of IEAE is a gray-scale image of size $M \times N$, denoted by $\mathbf{I} = \{I_{i,j}\}_{i=1,j=1}^{M,N}$. The whole plain-image is divided into blocks of size $p_1 \times p_2$ and is encrypted blockwise by IEAE. Let \mathbf{C} denotes the corresponding cipher-image. Then, the basic parts of IEAE can be described as follows.

- *The secret key*: non-negative integers $\omega_1, \omega_2, \mu_1, \mu_2$ used for array indexes; control parameter of Logistic map

$$x_n = \mu \cdot x_{n-1} \cdot (1 - x_{n-1}), \quad (1)$$

$\mu \in [3.9, 4]$; positive integer control parameters of generalized Arnold map

$$\begin{pmatrix} x_{n+1} \\ y_{n+1} \end{pmatrix} = \begin{pmatrix} 1 & a \\ b & 1 + a \cdot b \end{pmatrix} \cdot \begin{pmatrix} x_n \\ y_n \end{pmatrix} \bmod 1, \quad (2)$$

a and b , where $(x \bmod n) = x - n \cdot \lfloor x/n \rfloor$.

- *Public parameter*: iteration number R .

- *Initialization*:

1) Given an ECG signal $\mathbf{Z} = \{z_i\}_{i=1}^L$, its largest Lyapunov exponent, λ , is calculated by Wolf's algorithm proposed in [15]:

- *Step 1*: Transform the signal \mathbf{Z} into a sequence in an m -dimensional phase space, $\mathbf{Y} = \{Y_i\}_{i=1}^{L^*}$, where

$$Y_i = [z_{(i-1)m+1}, z_{(i-1)m+2}, \dots, z_{(i-1)m+m}],$$

$L^* = \lfloor L/m \rfloor$. Initialize indexes $k = 1$ and $t_k = 1$.

- *Step 2*: Calculate the distance

$$L_k = \|Y_{t_k} - Y_{t'_k}\|,$$

where $Y_{t'_k}$ is the directional nearest neighbor point of Y_{t_k} in the phase space, and the angle between $\overrightarrow{Y_{t_k} Y_{t'_{k-1}}}$ and $\overrightarrow{Y_{t_k} Y_{t'_k}}$, θ , is smaller than 30° when $k > 1$.

- *Step 3*: As the evolution and replacement procedure depicted in Fig. 1, incrementally increase the values of t_k and t'_k at the same time until the distance between Y_{t_k} and $Y_{t'_k}$ is larger than the threshold value ϵ . Then, set their current distance as L'_k , $k = k + 1$, and $t_k = t_{k-1}$.
- *Step 4*: Repeat *Step 2* and *Step 3* until $t_k > L^*$.
- *Step 5*: Calculate the largest Lyapunov exponent

$$\lambda = \frac{1}{t_k - 1} \sum_{k=1}^q \log_2 \left(\frac{L'_k}{L_k} \right), \quad (3)$$

where q is the total number of the replacement steps.

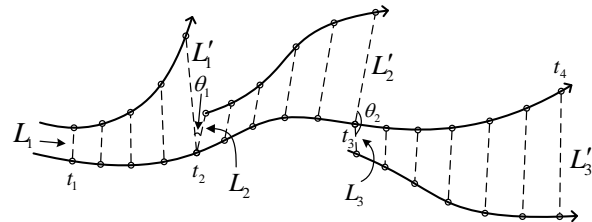


Figure 1: Schematic representation of the evolution and replacement procedure estimating the largest Lyapunov exponent from a phase space.

2) Iterate Eq. (1) P steps from initial condition $\bar{x}_0 = \text{Rem}(|\lambda| \cdot 10^8)$ with the control parameter μ and obtain integer sequence $\{\bar{x}_1, \bar{x}_2, \dots, \bar{x}_P\}$ via the conversion function

$$f(x) = (x \cdot 10^{14}) \bmod 256, \quad (4)$$

where $P = (p_1 \cdot p_2) + 256$, and $\text{Rem}(x)$ returns the fractional part of x .

3) Iterate Eq. (2) Q steps from $(x_0, y_0) = (|\lambda|, \text{Rem}(|\lambda| \cdot 10^5))$ and assign the obtained sequence $\{x_{r+1}, y_{r+1}, x_{r+2}, y_{r+2}, \dots, x_{r+MN/2}, y_{r+MN/2}\}$ converted by Eq. (4) into $M \times N$ matrix \mathbf{D} in the raster order, where $r = \bar{x}_{\mu_1}$, and $Q = r + MN/2$.

4) Assign sequence $\{\bar{x}_{\mu_3}, \bar{x}_{\mu_3+1}, \dots, \bar{x}_{\mu_3+p_1 \cdot p_2}\}$ into $p_1 \times p_2$ matrix \mathbf{C}_0 in the raster order, where

$$\mu_3 = \left(\sum_{i=1, j=1}^{p_1, p_2} I_{i,j} \right) \bmod 256 + 1, \quad (5)$$

• *The encryption procedure:*

– *Step 1:* Divide \mathbf{I} and \mathbf{D} into $r_1 \cdot r_2$ sub-blocks of size $p_1 \times p_2$, which is automatically selected from a fixed look-up table via random entries. Table 1 shows the table used for plain-images of size 256×256 . In this case, indexes

$$\begin{cases} q_1 = \lfloor \bar{x}_{\omega_1} \cdot 10^{14} \rfloor \bmod 3, \\ q_2 = \lfloor \bar{x}_{\omega_2} \cdot 10^{14} \rfloor \bmod 3. \end{cases} \quad (6)$$

For example, the block size is set as $(p_1, p_2) = (8, 16)$ if $(q_1, q_2) = (0, 1)$. If $p_1 \nmid M$ or $p_2 \nmid N$, some zero pixels are padded to the plain-image to make equations $M = r_1 \cdot p_1$ and $N = r_2 \cdot p_2$ both exist.

Table 1: Block sizes for plain-image of size 256×256 .

$q_1 \backslash q_2$	0	1	2
0	(8,8)	(8,16)	(8,32)
1	(16,8)	(16,16)	(16,32)
2	(32,8)	(32,16)	(32,32)

– *Step 2:* Encrypt the k -th block of plain-image \mathbf{I} , I_k , by

$$C_k = \begin{cases} (I_k + v \cdot D_k + C_{k-1}) \bmod 256 & \text{if } k < r_1 \cdot r_2; \\ (I_k + C_{k-1}) \bmod 256 & \text{if } k = r_1 \cdot r_2, \end{cases} \quad (7)$$

for $k = 1 \sim (r_1 \cdot r_2)$, where $v = \bar{x}_{\mu_2}$, and D_k denotes the k -th block divided in Step 1). To facilitate the

following description, we unify the two functions in Eq. (7) as the same form,

$$C_k = (I_k + v \cdot D_k + C_{k-1}) \bmod 256, \quad (8)$$

by setting $D_k \equiv 0$ if $k = r_1 \cdot r_2$.

• *Step 3:* Repeat the above step R times.

• *The decryption procedure* is the inverse version of Eq. (8), and operates

$$I_k = \begin{cases} (C_k - v \cdot D_k - C_{k-1}) \bmod 256 & \text{if } k < r_1 \cdot r_2; \\ (C_k - C_{k-1}) \bmod 256 & \text{if } k = r_1 \cdot r_2, \end{cases} \quad (9)$$

for $k = (r_1 \cdot r_2) \sim 1$.

3. Cryptanalysis of IEAE

In [14], the authors claimed that “the keystream generated is related to the plain-image, so it can effectively resist all kinds of differential attacks.” However, we argue that the statement is not true. Furthermore, we report the underlying mechanisms relating to the insecurity of some basic parts of IEAE.

3.1. Known-plaintext attack on IEAE

The known-plaintext attack is a cryptanalysis model assuming that the attacker can access a set of plaintexts and the corresponding ciphertexts encrypted by the same secret key. If an encryption scheme cannot withstand known-plaintext attack, every secret key should only be used only once in one encryption session, which would incur complex management of secret keys and very high cost. According to Kerckhoffs’s principle, an encryption algorithm should be secure even if everything about the algorithm, except the secret key, is public knowledge, which is reformulated by Shannon as “the enemy knows the system”. In [14], the authors claimed that “known-plaintext and chosen-plaintext attacks are infeasible for the proposed encryption algorithm” based on the sensitivity of matrix \mathbf{C}_0 on the change of plain-images, caused by the mechanism shown in Eq. (5). Actually, the sensitivity mechanism is cancelled due to the modulo addition in Eq. (5), which occurs with probability $1/256$ if every pixel in the plain-images is distributed uniformly.

Proposition 1. *Given any round number R , $\mathbf{D}' = \{D'_k\}_{k=1}^{r_1 r_2}$ is the equivalent secret key of IEAE for other plain-images generating the same value of μ_3 , where*

$$D'_k = \left(C_k - \underbrace{\sum_{h_1=1}^k \sum_{h_2=1}^{h_1} \dots \sum_{h_{R-1}=1}^{h_{R-2}} \sum_{i=1}^{k-h_{R-1}+1}}_{R \text{ times}} I_i \right) \bmod 256. \quad (10)$$

Proof. Observing Eq. (8), one has

$$\begin{aligned}
C_k &= (I_k + v \cdot D_k + C_{k-1}) \bmod 256 \\
&= (I_k + I_{k-1} + v \cdot (D_k + D_{k-1}) + C_{k-2}) \bmod 256 \\
&\vdots \\
&= \left(\sum_{i=1}^k I_i + v \cdot \sum_{i=1}^k D_i + C_0 \right) \bmod 256,
\end{aligned}$$

for any $k \in \{1, 2, \dots, r_1 \cdot r_2\}$. When $R = 2$ and the relationship between C_k and I_k becomes

$$\begin{aligned}
C_k &= \left(\sum_{i=1}^k I_i + v \cdot \sum_{i=1}^k D_i + C_0 + v \cdot D_k + C_{k-1} \right) \bmod 256 \\
&= \left(\sum_{i=1}^k I_i + v \cdot \sum_{i=1}^k D_i + C_0 + v \cdot D_k + \right. \\
&\quad \left. \sum_{i=1}^{k-1} I_i + v \cdot \sum_{i=1}^{k-1} D_i + C_0 + v \cdot D_{k-1} + C_{k-2} \right) \bmod 256 \\
&= \left(\sum_{h_1=1}^2 \sum_{i=1}^{k-h_1+1} I_i + v \cdot \sum_{h_1=1}^2 \sum_{i=1}^{k-h_1+1} D_i + 2C_0 + \right. \\
&\quad \left. v \cdot \sum_{i=k-1}^k D_i + \dots + I_1 + v \cdot D_1 + C_0 \right) \bmod 256, \\
&= \left(\sum_{h_1=1}^2 \sum_{i=1}^{k-h_1+1} I_i + v \cdot \sum_{h_1=1}^2 \sum_{i=1}^{k-h_1+1} D_i + v \cdot \sum_{i=1}^k D_i + k \cdot C_0 \right) \bmod 256.
\end{aligned}$$

As for any value of round number R , the relationship can be similarly derived:

$$C_k = \left(\underbrace{\sum_{h_1=1}^k \sum_{h_2=1}^{h_1} \dots \sum_{h_{R-1}=1}^{h_{R-2}} \sum_{i=1}^{k-h_{R-1}+1}}_{R \text{ times}} I_i + D'_k \right) \bmod 256, \quad (11)$$

where

$$\begin{aligned}
D'_k &= \left(v \cdot \left(\underbrace{\sum_{h_1=1}^k \sum_{h_2=1}^{h_1} \dots \sum_{h_{R-1}=1}^{h_{R-2}} \sum_{i=1}^{k-h_{R-1}+1}}_{R \text{ times}} D_i \right. \right. \\
&\quad \left. \left. + \underbrace{\sum_{h_1=1}^k \sum_{h_2=1}^{h_1} \dots \sum_{h_{R-2}=1}^{h_{R-3}} \sum_{i=1}^{k-h_{R-2}+1}}_{R-1 \text{ times}} D_i + \dots + \sum_{i=1}^k D_i \right) \right. \\
&\quad \left. + \underbrace{\sum_{h_1=1}^k \sum_{h_2=1}^{h_1} \dots \sum_{h_{R-3}=1}^{h_{R-4}} \sum_{i=1}^{k-h_{R-3}+1}}_{R-2 \text{ times}} i \cdot C_0 \right) \bmod 256,
\end{aligned}$$

From Eq. (11), one can see that the mask image $\mathbf{D}' = \{D'_k\}_{k=1}^{r_1 r_2}$ can work as the equivalent key of IEAE, which completes the proof of this proposition. \square

Given one pair of plain-image and the corresponding cipher-image, a mask image can be constructed as Proposition 1, which can be used to decrypt a cipher-image when the following two conditions hold at the same time: 1) it is encrypted by IEAE with the same secret key and public parameter as the given cipher-image; 2) its corresponding plain-image can generate the same value of μ_3 as the given plain-image. To check the validity of the proposed attack, we performed a number of experiments with some secret keys and more than 256 plain-images of size 512×512 . When the secret key and parameter are set as [14], namely $a = 1$, $b = 1$, $\omega_1 = 50$, $\omega_2 = 50$, $\mu = 3.999$, $\mu_1 = 20$, $\mu_2 = 15$, and $R = 3$, the plain-image “Lenna” and its results of encryption and decryption are shown in Fig. 2a), b), and c), respectively. A number of cipher-images encrypted with the same secret key as that of Fig. 2b) were decrypted by using the equivalent secret key obtained by the above attack, which is shown in Fig. 2e). Among them, the cipher-image shown in Fig. 2d) was successfully decrypted since the corresponding plain-image shown in Fig. 2f) can generate the same μ_3 as the plain-image “Lenna” by Eq. (5).

3.2. Security defects of IEAE

Using IEAE as a representative example, we analyze here the underlying mechanisms for its security defects, which also exist in many other image encryption schemes.

- The real structure of Logistic map in digital computer

In a finite-precision digital computer, dynamics of any chaotic maps satisfying a well-known chaos definition

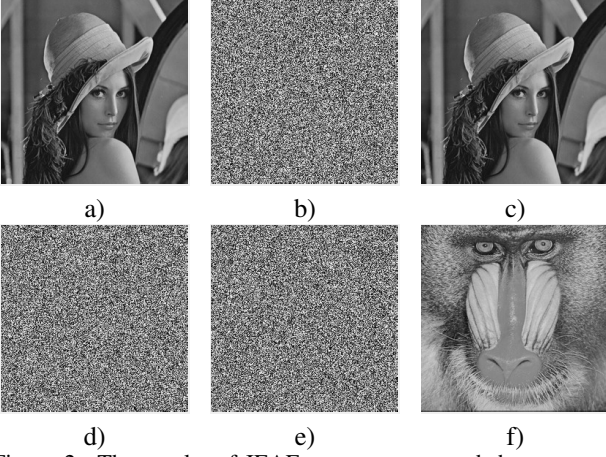


Figure 2: The results of IEAE cryptosystem and the proposed known-plaintext attack method: a) “Lenna”; b) encrypted “Lenna”; c) decrypted “Lenna”; d) encrypted “Baboon” with the same secret key; e) mask image \mathbf{D}' ; f) the breaking result of the encrypted “Baboon.”

in the infinite domain will definitely be degraded. Reliability of numerical solution of some chaotic dynamical systems is questionable [16]. Given an arithmetical domain (all possible representable numbers) and a rounding method, the *functional graph* of a chaotic map is determined. Just as [14, Fig. 1], a great number of research papers use the change trend of the positive Lyapunov exponent of digital chaotic maps with respect to control parameters to demonstrate complex degree of their dynamics. The metric only measures the maps from the macroscopic perspective. Actually, the calculated Lyapunov exponent in the digital domain is the change trend of the underlying functional graph along some evolution orbits (paths). So, some subtle properties of the digital chaotic map are omitted [17], such as short period cycles. To show this point, Fig. 3 depicts the functional graph of Logistic map with $\mu = 61/2^4$ in the arithmetic domain $\{0, 1, 2, \dots, 2^6\}$ under three quantization methods. Some small-sized connected components are omitted with a relatively high probability, which may lead to security defects of the supported system. Note that the structure of the functional graph of Logistic map implemented in a high precision is very similar to that in a lower precision [17]. Figure 4 presents the functional graph of Logistic map in a 9-bit floating-precision domain.

- Low efficiency of the method generating PRNS

In the field of image encryption, many schemes use

$$f_n(x) = f(10^m \cdot x) \bmod D \quad (12)$$

to convert a floating-point number into an n -bit integer number, where $f(x)$ is a quantization function, e.g. ceil, and floor. In computer, complexity of multiplication of two s -bit binary numbers is $O(s^\alpha)$, where $\alpha \in (1.35, 2]$ depending on the specific multiplication algorithm, e.g., Booth’s algorithm and Karatsuba algorithm. As

$$10^m = (2 \cdot (2^2 + 1))^m = \sum_{i=0}^m \binom{m}{i} \cdot 2^{3m-2i},$$

the number of “1” in the binary representation of 10^m , n_0 , is largely proportional to m . In a machine adopting the “shift and add” algorithm, the computational complexity is proportional to n_0 . Figure 5 depicts how the binary length of 10^m , $\lceil \log_2(10^m) \rceil = \lceil m \log_2(10) \rceil$, and n_0 changes with respect to m when $m \in [1, 50]$. As for Eq. (4) and Eq. (6), one has $m = 14$, $n_0 = 17$, and only the eight and two least significant bits are adopted, respectively. So, computations on most computed bits are wasted.

- Period behavior of the generalized Arnold map

In e -bit fixed-precision arithmetical domain, Eq. (2) is equivalent to

$$\begin{pmatrix} x'_{n+1} \\ y'_{n+1} \end{pmatrix} = \begin{pmatrix} 1 & a' \\ b' & 1 + a' \cdot b' \end{pmatrix} \cdot \begin{pmatrix} x'_n \\ y'_n \end{pmatrix} \bmod 2^e, \quad (13)$$

where $a' = a \bmod 2^e$, $b' = b \bmod 2^e$, $x'_n = \lfloor x_n \cdot 2^e \rfloor$, and $y'_n = \lfloor y_n \cdot 2^e \rfloor$. To visualize the real structure of the generalized Arnold map, we depict its functional graph with two sets of parameters in Fig. 6, where the number in each node denotes

$$z_n = x'_n + (y'_n \cdot 2^e),$$

and $e = 4$. The whole graph shown in Fig. 6a) is composed of 8 connected components (CC) of period 16, 8 CC of period 8, 8 CC of period 4, 11 CC of period 2, and 8 self-connected nodes. So, the support of [14, Fig. 2] on random behavior of the generalized Arnold map is groundless. Actually, it only plots a short orbit (path) in a connected component obtained in the digital computer. In addition, although the maximal Lyapunov exponent of the generalized Arnold map is positive, it is a metric measuring the overall dynamics of a system, which may fail to demonstrate complex dynamics (randomness) of the system in a local domain.

- Incapability of the test metrics adopted by IEAE

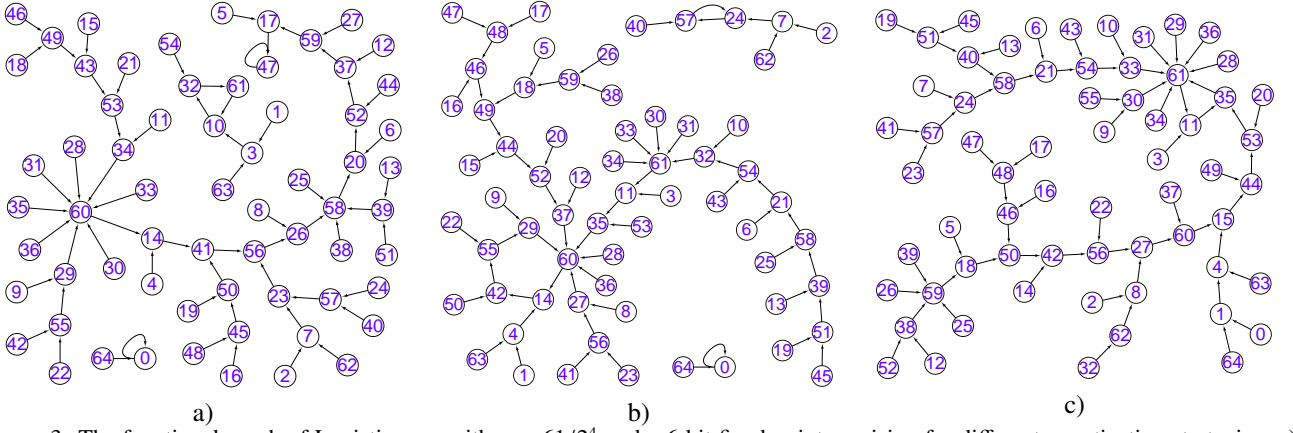


Figure 3: The functional graph of Logistic map with $\mu = 61/2^4$ under 6-bit fixed-point precision for different quantization strategies: a) floor; b) round; c) ceil, where the number i in each node denotes value $i/2^6$.

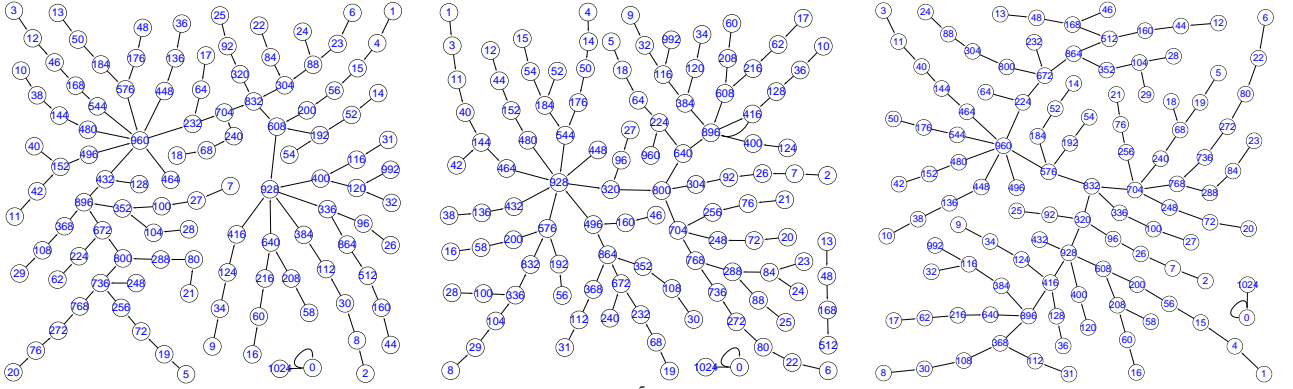


Figure 4: The functional graph of Logistic map with $\mu = 123/2^5$ under 9-bit floating-point precision, where significant digits (the significant) and exponent both occupy 4 bits and the number i in each node denotes value $i/2^{10}$.

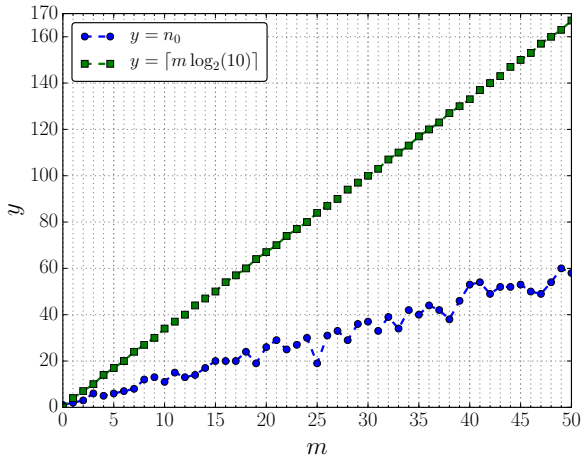


Figure 5: The bit length of 10^m and the number of “1” in its binary presentation.

- **Key Space and Sensitivity:** The size of the key space of IEAE is bounded by the number of available of

ECG signals, which incur complex burdens of secure storage and transmission of the sensitive information and may violate the availability principle of security [18]. Just like the dynamics of any chaotic system are degenerated in digital world [13], the sensitivity of digitized ECG signals with respect to a sampled person and time also worsens to some extents. Furthermore, due to the addition and division in Eq. (3), totally different ECG signals may own the same largest Lyapunov exponent. So, the statement in [14], “ECG is like a one-time keypad—different people will have different ECGs, so the keys will not be used twice”, is questionable.

- **Histograms:** As shown in [2], an attacker cannot efficiently obtain some meaningful information from the uniform histogram of pixels, but can learn important statistic information about the plain-image from the histogram of bits. So, changing the objects of histogram may make the statement in [14, Fig. 6]

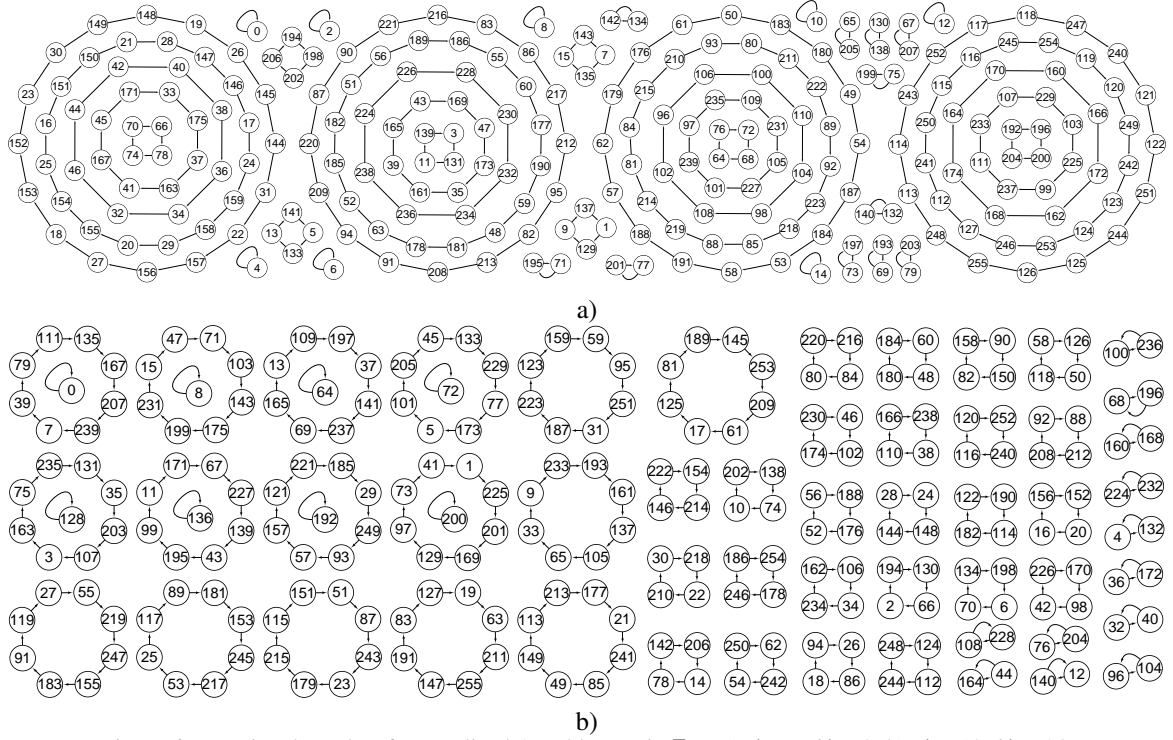


Figure 6: Functional graphs of generalized Arnold maps in \mathbb{Z}_2^4 : a) $a' = 7, b' = 8$; b) $a' = 12, b' = 14$.

become invalid.

- **Differential Attack:** Differential attack is to find information about the secret key of an encryption scheme by studying how differences between plaintexts can affect the resultant difference between the corresponding ciphertexts, which is unrelated to the index *UACI* measuring how plaintext influences the corresponding ciphertext.
- **Correlation Coefficients:** Weak correlation among adjacent pixels is only a necessary (not sufficient) condition for an invisible cipher-image, which is only related with the capability resisting statistical analysis from a single cipher-image. In fact, position permutation is a sufficient way to reduce correlation coefficients among neighbouring elements in a plain-image [4].
- **Efficiency:** In [14], it is claimed that “implementing encryption using the proposed algorithm is fast”. In fact, the fast running speed of IEAE is built on the simple linear encryption function by sacrificing security. Note that the computational load spent on direct encryption of a plain-image is proportional to the number of plain-bytes and is unrelated with the block size. Even worse, a substantial part of the limited computational load of IEAE is wasted in the

processes generating pseudorandom binary sequences. Among them, the computation of the largest Lyapunov exponent involves very complex operations (see Sec. 2 or [15]) and the final computational complexity depends on the specific used algorithmic. Furthermore, Wolf’s method is also very dependant on the length of the time series and in parameters selection (i.e., the embedding dimension and the time delay). Such a dependence could incur differences between similar configurations in different computers or setups, which may lead to slightly different initial conditions of Logistic map. For example, the same configuration for computing logarithm in Eq. (3) has to be adopted by both secure communication sides. All these dependency problems erode the practicality of IEAE. To obtain a satisfying balance between efficiency, usability, and security, selecting some important data in the compressing domain of a plain-image for encryption is a practical approach.

4. Conclusion

This paper analyzed security of an image encryption algorithm based on autoblocking and electrocardiography, and showed that the algorithm was very weak against the

known-plaintext attack. Security defects in the analyzed algorithm were summarized to inform designers of image encryption schemes about common pitfalls and help them improve security levels protecting image data in the current cyberspace.

Acknowledgements

This work was supported by the National Natural Science Foundation of China (no. 61772447, 61532020).

References

- [1] L. Bao, S. Yi, and Y. Zhou, "Combination of sharing matrix and image encryption for lossless (k, n) -secret image sharing," *IEEE Transactions on Image Processing*, vol. 26, no. 12, pp. 5618–5631, Dec 2017.
- [2] C. Li, D. Lin, and J. Lü, "Cryptanalyzing an image-scrambling encryption algorithm of pixel bits," *IEEE MultiMedia*, vol. 3, pp. 64–71, 2017.
- [3] E. Y. Xie, C. Li, S. Yu, and J. Lü, "On the cryptanalysis of Fridrich's chaotic image encryption scheme," *Signal Processing*, vol. 132, pp. 150–154, 2017.
- [4] G. Alvarez and S. Li, "Some basic cryptographic requirements for chaos-based cryptosystems," *International Journal of Bifurcation and Chaos*, vol. 16, no. 8, pp. 2129–2151, 2006.
- [5] P. Peris-Lopez, L. González-Manzano, C. Camara, and J. M. de Fuentes, "Effect of attacker characterization in ECG-based continuous authentication mechanisms for internet of things," *Future Generation Computer Systems*, vol. 81, pp. 67–77, 2018.
- [6] Z. Zhang, H. Wang, A. V. Vasilakos, and H. Fang, "ECG-cryptography and authentication in body area networks," *IEEE Transactions on Information Technology in Biomedicine*, vol. 16, no. 6, pp. 1070–1078, Nov 2012.
- [7] T. Ma, P. L. Shrestha, M. Hempel, D. Peng, H. Sharif, and H.-H. Chen, "Assurance of energy efficiency and data security for ECG transmission in basns," *IEEE Transactions on Biomedical Engineering*, vol. 59, no. 4, pp. 1041–1048, Apr 2012.
- [8] M. Barni, P. Failla, R. Lazzeretti, A.-R. Sadeghi, and T. Schneider, "Privacy-preserving ECG classification with branching programs and neural networks," *IEEE Transactions on Information Forensics and Security*, vol. 6, no. 2, pp. 452–468, Jun 2011.
- [9] S. I. Safie, J. J. Soraghan, and L. Petropoulakis, "Electrocardiogram (ECG) biometric authentication using pulse active ratio (par)," *IEEE Transactions on Information Forensics and Security*, vol. 6, no. 4, pp. 1315–1322, DEC 2011.
- [10] C.-K. Chen, C.-L. Lin, C.-T. Chiang, and S.-L. Lin, "Personalized information encryption using ECG signals with chaotic functions," *Information Sciences*, vol. 193, pp. 125–140, 2012.
- [11] D. Arroyo, G. Alvarez, and V. Fernandez, "On the inadequacy of the logistic map for cryptographic applications," <https://arxiv.org/abs/0805.4355>, 2008.
- [12] G. Alvarez, J. M. Amigó, D. Arroyo, and S. Li, "Lessons learnt from the cryptanalysis of chaos-based ciphers," in *Chaos-Based Cryptography*. Springer, 2011, pp. 257–295.
- [13] Q. Wang and et al., "Theoretical design and FPGA-based implementation of higher-dimensional digital chaotic systems," *IEEE Transactions on Circuits and Systems I: Regular Papers*, vol. 63, no. 3, pp. 401–412, 2016.
- [14] G. Ye and X. Huang, "An image encryption algorithm based on autoblocking and electrocardiography," *IEEE MultiMedia*, vol. 23, no. 2, pp. 64–71, 2016.
- [15] A. Wolf, J. B. Swift, H. L. Swinney, and J. A. Vastano, "Determining Lyapunov exponents from a time series," *Physica D: Nonlinear Phenomena*, vol. 16, no. 3, pp. 285–317, 1985, www.mathworks.com/matlabcentral/fileexchange/48084.
- [16] R. Lozi, "Can we trust in numerical computations of chaotic solutions of dynamical systems?" in *Topology and dynamics of Chaos: In celebration of Robert Gilmore's 70th birthday*. World Scientific, 2013, pp. 63–98.
- [17] C. Li, B. Feng, S. Li, J. Kurths, and G. Chen, "Dynamic analysis of chaotic maps as complex networks in the digital domain," <https://arxiv.org/pdf/1410.7694>, 2017.
- [18] W.-S. Yap, R. C.-W. Phan, B.-M. Goi, W.-C. Yau, and S.-H. Heng, "On the effective subkey space of some image encryption algorithms using external key," *Journal of Visual Communication and Image Representation*, vol. 40, pp. 51–57, 2016.